Journal of Applied Polymer Science

Synthesis and Characterization of a Magnetic Hybrid Material Consisting of Iron Oxide in a Carboxymethyl Cellulose Matrix

Juan Francisco Luna-Martínez,[1] Edgar Reyes-Melo,[1,2] Virgilio González-González,[1,2] Carlos Guerrero-Salazar,[1,2] Alejandro Torres-Castro,[1,2] Selene Sepúlveda-Guzmán[1,2]

[1]UANL-FIME, Programa Doctoral en Ingeniería de Materiales, Avenida Universidad s/n Cd.Universitaria San Nicolás de los Garza, Nuevo León 66450, México

[2]CIIDIT-PIIT, Nueva Autopista al Aeropuerto Internacional Monterrey Km 10, Apodaca, Nuevo León, México

Correspondence to: E. Reyes-Melo (E-mail: mreyes@gama.fime.uanl.mx)

ABSTRACT: A magnetic hybrid material (MHM), consisting of iron-oxide nanoparticles (4 nm) embedded in sodium carboxymethyl cellulose (Na-CMC) matrix was synthesized. The MHM synthesis process was performed in two stages. First, a precursor hybrid material (Fe(II)-CMC) was synthesized from two aqueous solutions: Na-CMC solution and $FeCl_2$ solution. In the second stage, the precursor hybrid material was treated with H_2O_2 under alkaline conditions to obtain the MHM. The results obtained from X-ray diffraction show that the crystalline structure of iron oxide into MHM corresponds to maghemite or magnetite phase. Conversely, the results obtained from Fourier transform infrared (FTIR) spectroscopy reveal that the polymeric matrix (Na-CMC) preserves its chemical structure into the MHM. Furthermore, in FTIR spectra are identified two characteristic bands at 570 and 477 cm^{-1} which can be associated to maghemite phase. Images obtained by high resolution transmission electron microscopy and bright field scanning transmission electron microscope show that iron-oxide nanoparticles are embedded in the Na-CMC. Magnetic properties were measured at room and low temperature using a quantum design MPMS SQUID-VSM magnetometer. Diagrams of magnetization versus temperature show that iron-oxide nanoparticles embedded in Na-CMC have a superparamagnetic-like behavior. © 2012 Wiley Periodicals, Inc. J. Appl. Polym. Sci. 000: 000–000, 2012

KEYWORDS: nanocomposite; magnetic polymers; nanoparticles; nanotechnology

Received 9 April 2010; accepted 6 April 2012; published online
DOI: 10.1002/app.37892

INTRODUCTION

During the past two decades, researchers have paid a lot of attention to magnetic iron-oxide nanoparticles.[1–4] Several applications have been reported, such as, high density data magnetic recording media,[5] catalysis,[6] magnetic fluids,[7] image-intensifying agents for nuclear magnetic resonance imaging,[8] medical diagnosis, controlled drug delivery, and magnetic-induced cancer therapy.[9,10] Magnetic nanoparticles can be synthesized by methods, such as, sol–gel,[11,12] coprecipitation,[13,14] and microemulsion,[15] among others. Nevertheless, during and after the synthesis, the high surface energy of nanoparticles promotes a tendency to form aggregates.[16] This problem can be avoided by encapsulating the nanoparticles in a matrix material.[17] Mesoporous silica[18] and zeolites[19] have been used as a matrix in the formulation of magnetic composites; however, these ceramic materials are limited due to their poor malleability, reason why they cannot be put under processes of change of form. In this sense, and motivated mainly by the excellent manageability, flexibility, and transparency[20] of the polymeric materials, a significant amount of research has been focused on the incorporation of magnetic nanoparticles into polymeric matrices. For this case, different methods can be used, for example, nanoparticles can be synthesized *in situ* inside the polymeric matrix[21] that usually have functional groups that can form coordination bonds with metallic ions.[22] In a recent work,[23] it has reported that the synthesis of ZnS nanoparticles with a blende structure and a particle size in the range of few nanometers are well dispersed in the sodium carboxymethyl cellulose (Na-CMC) films. The Na-CMC is a cellulose derivative with the carboxymethyl group bounded to the hydroxyl group of the anhydroglucose unit (Figure 1). Because of its chemical structure, Na-CMC can form coordinate bonds with divalent ions without loss of its process ability.[24]

For several technological applications, the degree of substitution (DS) value (average number of carboxymethyl groups per each

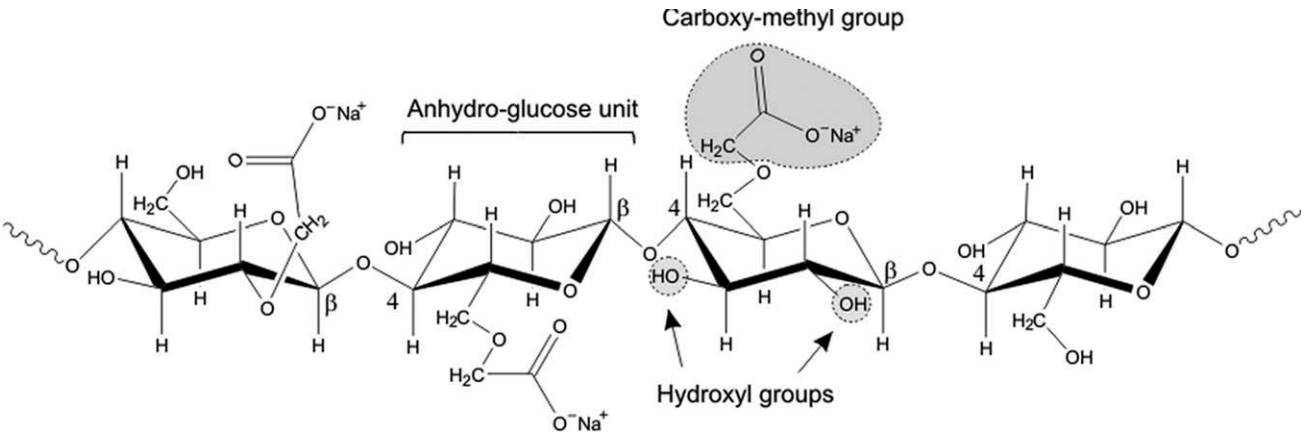

Figure 1. A representative segment of Na-CMC polymeric chain.

10 units of anhydroglucose) must be less than 3. This is because in those cases, the biopolymer has high solubility in cold and hot water, high water retention, high chemical resistance to oils, fats and organic solvents and a certain degree of adhesiveness, and film forming ability. These characteristics and its nontoxicity have made Na-CMC suitable for applications in many foodstuffs formulations. Na-CMC has also been widely used as a carrier for bone grafting.[25,26] In this work, we report the *in situ* synthesis and characterization of iron-oxide/carboxymethyl cellulose magnetic nanocomposite. The originality of this work is based on which the iron-oxide nanoparticles are synthesized *in situ* from a hybrid material (Fe(II)-CMC) as precursor. The structural characterization of iron-oxide/carboxymethyl cellulose magnetic nanocomposite was made by X-ray diffraction (XRD) and Fourier transform infrared spectroscopy (FTIR). The morphological analysis was performed by scanning transmission electron microscope (STEM) and high resolution transmission electron microscopy (HRTEM). In addition, we studied the magnetic behavior by means of magnetization measurements using both field cooling (FC) and zero FC (ZFC) analysis.

EXPERIMENTAL

Na-CMC with a 0.7 DS was used in this work. The Na-CMC was supplied by Sigma-Aldrich Química S. A. Toluca, Estado de México, México, and it is classified as of "medium viscosity": 400–800 cP 2% in H_2O (25°C). As precursor salt for Fe^{+2}, ferrous chloride tetrahydrate ($FeCl_2{\cdot}4H_2O$, 99.9%) was used and it was supplied by Fermont (Distributed in Mexico for Fisher Scientific de México, Monterrey, Nuevo León, México). Sodium hydroxide (NaOH, 97%) was used to obtain alkaline conditions, and it was supplied by Fermont. Finally, the hydrogen peroxide (H_2O_2, 3%) used was supplied by Zuum (Cd. México, D.F., México). All materials were used as-received for the synthesis of the magnetic hybrid material (MHM) consisting of iron oxide in a CMC matrix.

The process to obtain the MHM was performed in two stages. In the first one, it was synthesized as a precursor hybrid material (Fe(II)-CMC). In the second stage, the precursor hybrid material was used to synthesize iron-oxide nanoparticles into CMC matrix.

Stage 1: 1 g of Na-CMC was dissolved into 70 mL of distilled water and then Na-CMC/H_2O was stirred for 5 h (solution 1). Conversely, a solution of 20 mL 0.25*M* $FeCl_2{\cdot}4H_2O$ using distilled water as solvent was prepared (solution 2). Solutions 1 and 2 were mixed and stirred for 4 h. The final mixture (solution 1/2) was poured in a glass Petri dish. Then, the glass Petri dish was put on a hot plate at 40°C for 24 h to eliminate the solvent (water) by natural convection drying. After that precursor hybrid material (Fe(II)-CMC) was obtained.

Stage 2: In this experimental part, the precursor hybrid material was submerged in a solution 6.7*M* NaOH at 40°C obtaining a rapid change in color, from brown to black. After that 30 mL of H_2O_2 (40°C) was added to the "black material," observing a color change from black to brownish. Finally, the "brownish material" was washed several times with distilled water and ethanol to eliminate the residual products (NaOH and Cl^-). After that the MHM was obtained. Both the precursor hybrid material (Fe(II)-CMC) and MHM were studied by XRD and FTIR analysis.

X-ray analysis was performed using a Siemens D-500 diffractometer with Cu Kα radiation at 35 kV and 25 mA at a scan rate of 0.03° (2θ)/s. In both cases, the samples were pulverized for X-ray analysis.

The IR spectra were obtained using a FTIR spectrometer (Perkin Elmer Spectrum GX) in transmittance mode, scanning 32 times at 4 cm^{-1} resolution from 400 to 4000 cm^{-1}. For this case, two samples were pulverized and mixed with KBr to make up pellet samples.

The morphology and structure of MHM were studied by HR-TEM and STEM. The analysis of transmission electron microscopy was done in a Jeol 2010 TEM, operating at 200 kV. The specimen was prepared by dispersing the MHM powder in acetone using an ultrasonic bath and placing an aliquot of the dispersion onto lacey carbon-coated TEM grid. The STEM was done using a Hitachi S-5500 In-lens field emission scanning electron microscope; in this case, the samples were prepared with the same technique used for the TEM analysis samples.

Magnetic properties were measured at room and low temperature using a quantum design MPMS SQUID-VSM

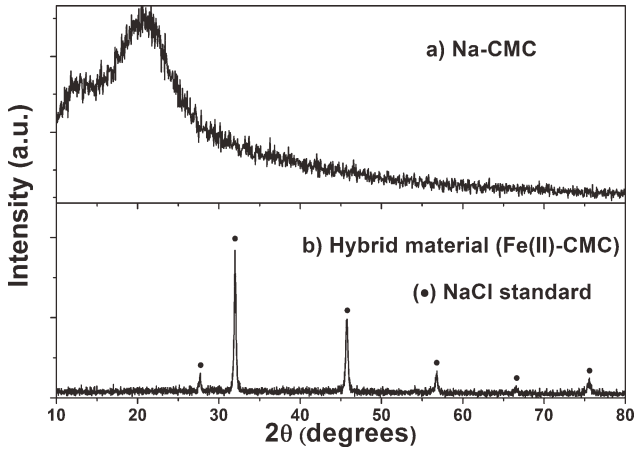

Figure 2. XRD patterns for (a) as received Na-CMC and (b) hybrid material (Fe(II)-CMC), (•) sodium chloride standard.[27]

magnetometer. The specimen (powder nanocomposite) was encapsulated for its analysis.

RESULTS AND DISCUSSION

The microstructure of the precursor hybrid material (Fe(II)-CMC) was studied by X-ray and FTIR analysis. Figure 2(a) shows the X-ray pattern obtained for Na-CMC sample. A typical broad band is observed at lower 2θ values (15°–25°), which is typical result for an amorphous polymer. Conversely, Figure 2(b) corresponds to the diffraction pattern of Fe(II)–CMC. This diagram does not show peaks associated to the $FeCl_2{\cdot}4H_2O$. However, Figure 2(b) shows several diffraction peaks at 27°, 32°, 46°, 57°, 67°, and 76°, and they are associated to NaCl crystals.[27] These results suggest that $FeCl_2{\cdot}4H_2O$ was completely dissolved in the Na-CMC.[28] The existence of NaCl is associated to chemical reaction occurring between Cl^- and Na^+.

With respect to the infrared analysis, the comparison between the FTIR spectrum of Na-CMC and the FTIR spectrum of the precursor hybrid material allows us to identify if the vibration

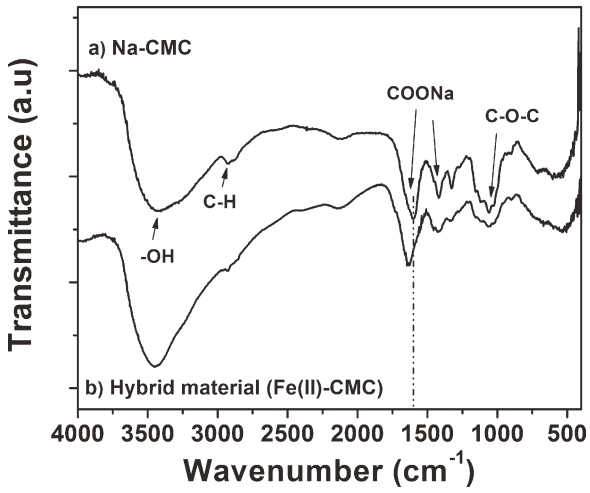

Figure 3. IR Spectra of (a) Na-CMC alone and (b) the precursor hybrid material (Fe(II)-CMC).

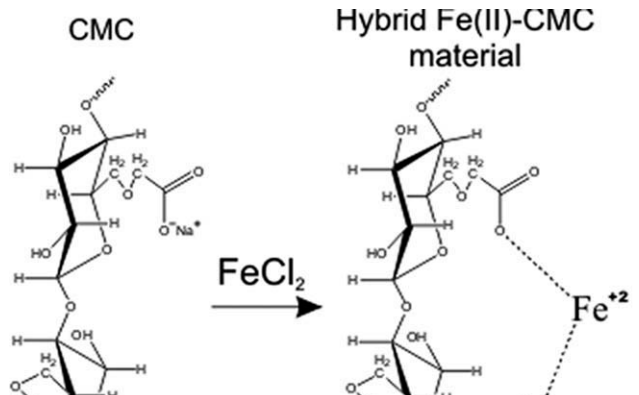

Figure 4. Schematic representation of the precursor hybrid material (Fe(II)-CMC) formation.

modes of the chemical groups of the Na-CMC are modified or not due to the presence of Fe^{+2} and Cl^{-1} into the precursor hybrid material. The Na-CMC FTIR spectrum [Figure 3(a)] shows the characteristic broad band of —OH groups at 3500 cm^{-1}, the C—H stretching vibration band at 2925 cm^{-1}, the asymmetric stretching band of ether groups at 1058 cm^{-1}, and the associated bands of carboxyl groups at 1600 and 1417 cm^{-1}. Figure 3(b) shows FTIR spectrum of the precursor hybrid material; it is observed that the band associated to carboxyl groups is shifted to higher wavenumbers, around 1633 cm^{-1}. This fact is related to chemical interactions between Fe^{+2} and the carboxyl groups of the Na-CMC (the electronegativity of Fe^{+2} ions is twice that of Na^{+1}). Figure 4 is a representative scheme showing interaction between Fe^{+2} and carboxyl groups of Na-CMC. These FTIR results corroborate that Fe^{+2} ions are completely dissolved into the CMC obtaining the precursor hybrid material.

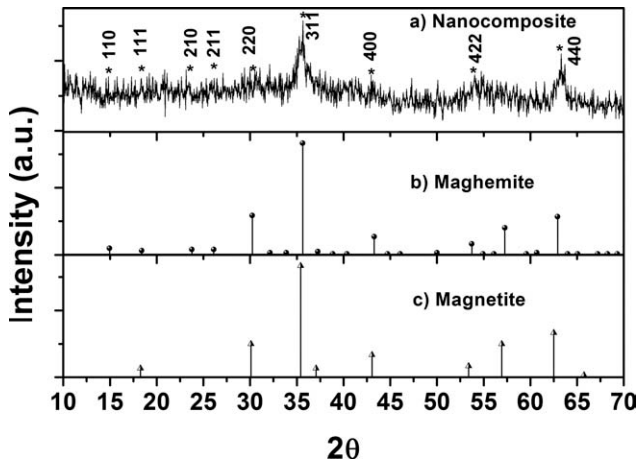

Figure 5. XRD patterns for (a) the obtained iron oxide/CMC nanocomposite or MHM, (b) maghemite, and (c) magnetite standards.

Table I. Summary Data for Calculated *d* [*d*(exp)] Spacing from Experimental X-ray Patterns [2θ (exp)] and from ICDD-data base for Iron Oxide [*d*(γ-Fe2O3)], [*d*(Fe3O4)], and Miller Indices, Respectively

Exp Hkl	*d*(Computed)	*d*(γ-Fe_2O_3)	*d*(Fe_3O_4)
*110	0.5921	0.5918	-
*111	0.4830	0.4822	0.4852
*210	0.3743	0.374	-
*211	0.3411	0.3411	-
*220	0.2952	0.2953	0. 2967
*311	0.2516	0.2517	0.2532
*400	0.2090	0.2088	0.2099
*422	0.1705	0.1704	0.1714
*440	0.1475	0.1475	0.1484

Lengths are Measured in Nanometers.
*Peaks showed in Fig. 5a.

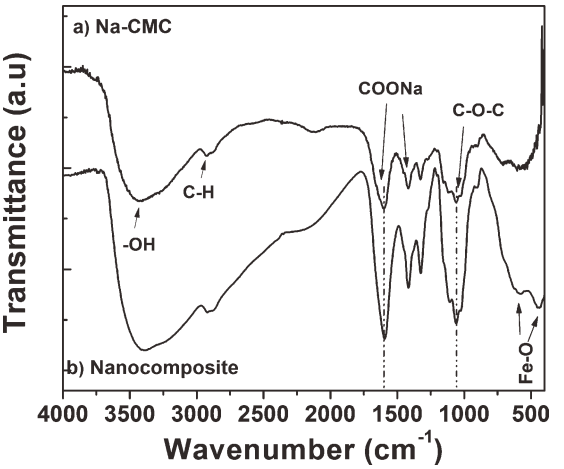

Figure 6. IR Spectra of (a) Na-CMC alone and (b) iron oxide/CMC nanocomposite or MHM.

After chemical treatment of the precursor hybrid material with H_2O_2 under alkaline conditions, its change in color was from black to brownish, this fact suggests the formation of iron-oxide nanoparticles embedded into the CMC matrix. To corroborate this fact, "brownish material" was studied by XRD. Figure 5(a) shows the diffraction pattern obtained. Diffraction peaks are identified in Figure 5(a) at 18.35°, 30.25°, 35.65°, 42.25°, 53.7°, and 62.95° that correspond to the (111), (220), (311), (400), (422), and (440) plane reflections of maghemite [Figure 5(b)][29] or magnetite [Figure 5(c)] crystalline structures.[30] However, peaks at 15°, 23.8°, and 26.1° are also identified in Figure 5(a). These diffraction peaks correspond to (110), (210), and (211) planes that are associated to maghemite phase. Using Bragg's law, for each diffraction peak of Figure 5(a), the lattice spacing *d* was calculated and compared with reported values in database of the International Centre for Diffraction Data. Table I shows *d* computed values and the reported values in ICDD data base for magnetite and maghemite phase. The computed *d* values are very close to the ICDD values for maghemite crystalline structure.[29] Conversely, from the experimental diffractogram [Figure 5(a)], it is also possible to compute the crystal size $<L>$ by Scherrer eq. (1)

$$< L >= \frac{0.89\lambda}{\beta \cdot \mathrm{Cos}\theta}, \qquad (1)$$

where λ is the wavelength of the incident X-rays, θ is the half of the diffraction angle 2θ in degrees, and β is the full width at half maximum of the diffraction peak.[31] The computed value

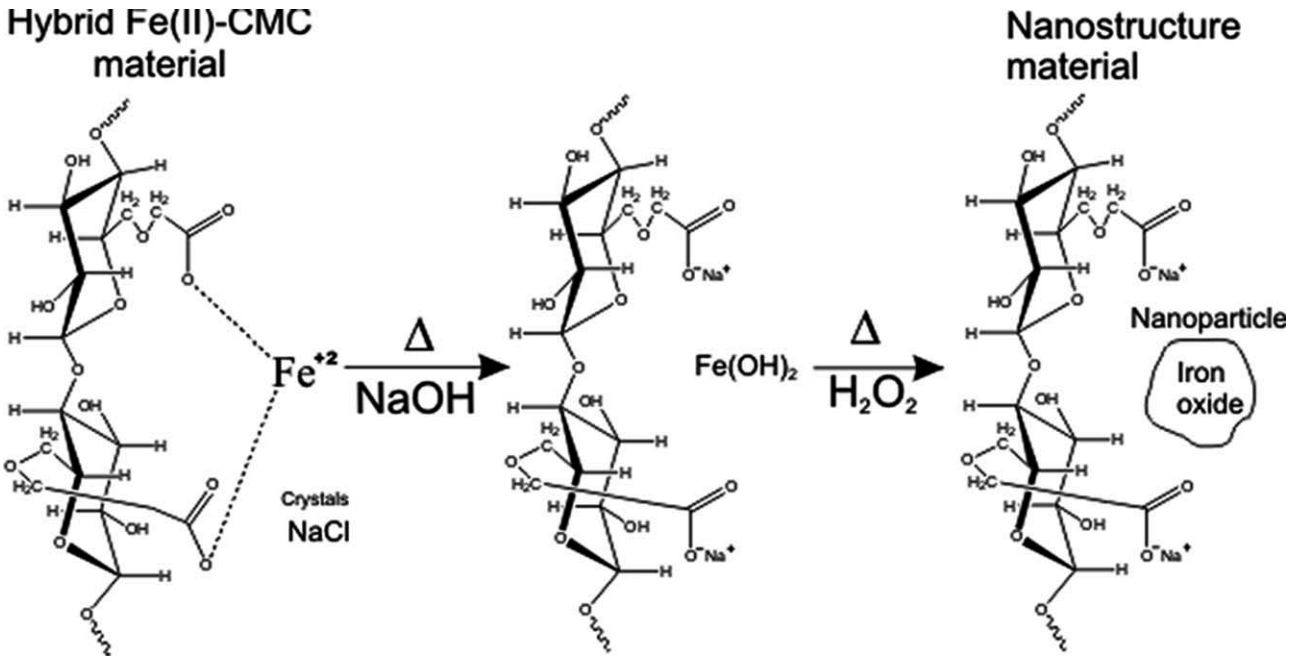

Figure 7. Schematic representation of the process used in the preparation of the iron oxide/CMC nanocomposite or MHM.

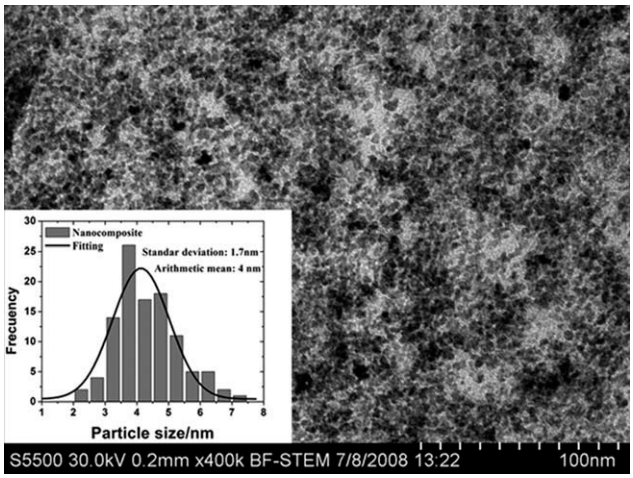

Figure 8. BF-STEM images of iron oxide/CMC nanocomposite or MHM.

$<L>$ obtained was 5.6 nm. These results suggest that iron-oxide nanoparticles are embedded in the CMC.

To obtain additional information about the chemical structure of the MHM, an FTIR spectroscopy analysis was performed [Figure 6(b)]. The FTIR spectrum obtained [Figure 6(b)] shows the characteristic bands of Na-CMC at 3500, 2925, and 1058 cm^{-1} already mentioned. In this case, unlike the FTIR spectrum of the precursor hybrid material [Figure 3(b)], the bands associated to the carboxyl groups remain at 1600 and 1417 cm^{-1} for the MHM [Figure 6(b)]. This result can be interpreted as a weak-chemical interaction between iron-oxide nanoparticles and the carboxyl groups of the Na-CMC. In addition, the band at 1600 cm^{-1} also suggests that during the iron-oxide precipitation, the sodium-carboxyl groups were again formed through the reaction of carboxyl groups (COO—) with Na^{+} of NaOH added to obtain alkaline conditions (Figure 7). It is important to remark here the presence of two peaks in the FTIR spectrum for MHM [Figure 6(b)], they are located at 570 and 437 cm^{-1} wavenumber. In Ref. 21, these bands were associated to the Fe—O bending vibrations of the maghemite iron-oxide phase.[21] These results are in agreement with those obtained through XRD analysis.

The size and morphology of iron-oxide nanoparticles into MHM were studied by STEM and HRTEM analysis. The STEM images (Figure 8) show a higher number of iron-oxide nanoparticles with sphere-like morphology. The average particle size of the iron oxide was measured using image analysis, and the frequency histogram shows a size of 4 nm (inset Figure 8), very similar to the previously computed value $<L>$ obtained using the Scherrer equation.

The HRTEM images of the iron-oxide nanoparticles are shown in Figure 9(a, b). The well-defined lattice fringes correspond to crystallographic plane of iron-oxide nanoparticles and they are identified in both figures. In addition, interplanar distances: 0.477, 0.332, 0.297, and 0.249 nm were computed from Figure 9(a, b). These computed values correspond to interplanar distances of (111), (211), (220), and (311) planes. These crystallographic planes are of maghemite crystalline structure, which is consistent with the XRD analysis. These interplanar distances are very close to the computed values, shown in Table I.

Finally, the magnetic behavior of the MHM was studied by magnetization measurements. Figure 10 shows the magnetization curve at room temperature (300 K). The saturation magnetization value (Ms) is 13.9 emu/g whereas both, remnant magnetization and coercivity (Hc) are undetectable. These last results are characteristics of a magnetic nanocomposite or MHM with superparamagnetic behavior.[32]

Conversely, Figure 11 presents the magnetization curve at 2 K. Under these conditions both coercitivity field and remnant magnetization values are different to zero. It can be seen that the corresponding values for the different magnetic parameters are 19.9 emu/g for saturation magnetization, 357 Oe for

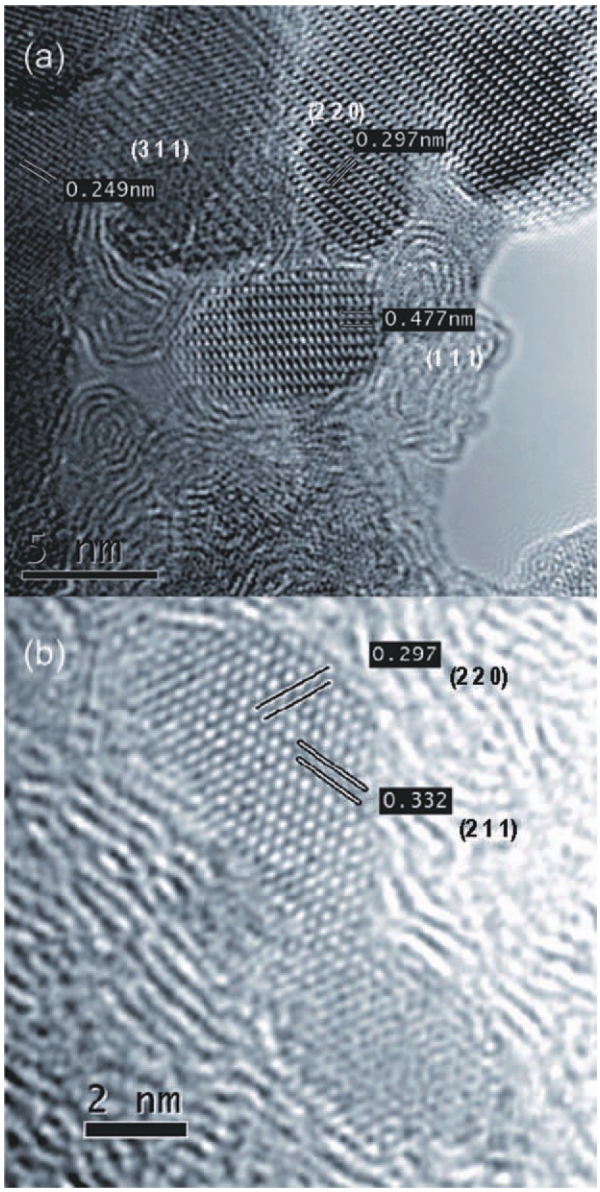

Figure 9. HRTEM images of iron oxide nanocrystals. [Color figure can be viewed in the online issue, which is available at wileyonlinelibrary.com.]

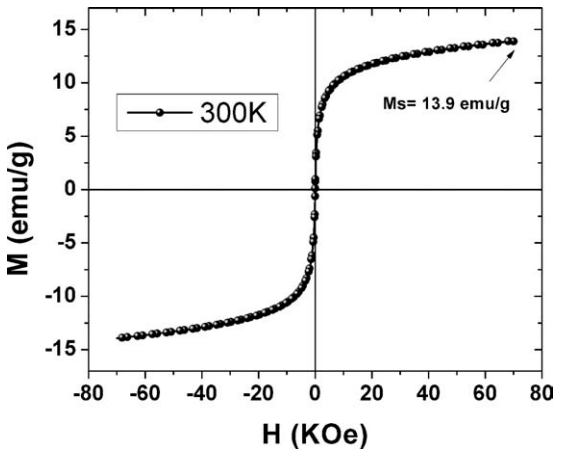

Figure 10. Magnetization curve for MHM at room temperature (70 kOe).

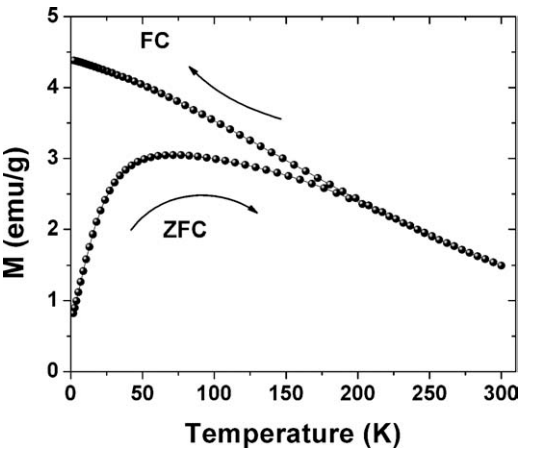

Figure 12. ZFC and FC magnetization curves at 100 Oe.

coercive field (Hc), and 6.14 emu/g for remanence value (Mr) (inset Figure 10); a ferromagnetic behavior appears when the magnetic analysis is performed below the blocking temperature (T_B).[33] To estimate the T_B for the MHM sample, FC and ZFC analyses were performed at a magnetic field of 100 Oe (Figure 12).

When the MHM sample is cooled at zero magnetic field, Figure 12 shows that the total magnetization is small, but not zero (it is ~20% of the maximum), as the magnetic particles are not fully random. When temperature increases, the nanoparticle magnetic moment is oriented with the external field increasing the total magnetization until it reaches a maximum at 71 K which is the value of the blocking temperature. At this temperature, the thermal energy becomes comparable to the energy gained by aligning the nanoparticle magnetic vector in the weak field. At this point, the transition from ferromagnetic to superparamagnetic behavior is observed.[34] When all nanoparticles are at the superparamagnetic relaxation state, above T_B, their magnetization follows Curie's law decreasing with increasing temperature.[35] In the case of FC, magnetization monotonically increases as the temperature decreases because the nanoparticles are cooled from room temperature under a magnetic field and the magnetization direction of all the nanoparticles is frozen in the field direction. The magnetization shows the maximum at 2 K in the FC process (Figure 12).

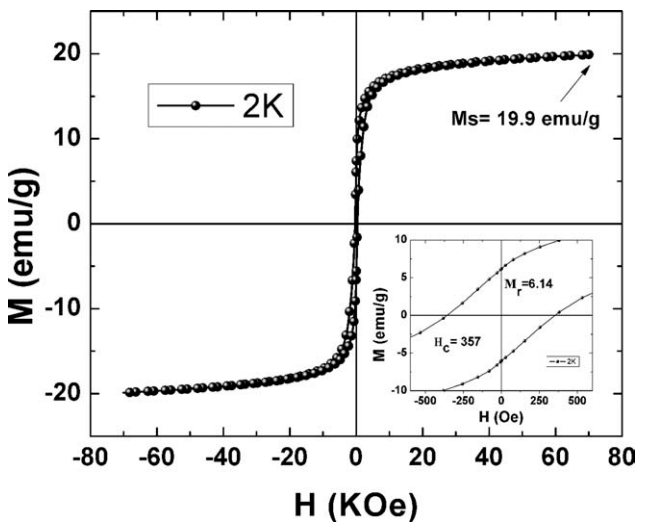

Figure 11. Magnetization curve for MHM at 2 K.

CONCLUSIONS

An MHM consisting of nanoparticles of iron oxide in a Na-CMC matrix was obtained. The synthesis of magnetic nanoparticles from the precursor hybrid material or Fe(II)-CMC was confirmed via XRD and FTIR analysis. The iron-oxide nanoparticles are embedded in the polymer Na-CMC matrix and their measured size was around 4 nm, having a nearly spherical morphology. The analysis of the magnetic properties of the MHM shows a superparamagnetic behavior at room temperature changing to ferromagnetic below 71 K, the blocking temperature. Our results suggest that *in situ* precipitation of nanoparticles in the precursor hybrid material (Fe(II)-CMC) is a promising route to the production of MHM.

ACKNOWLEDGMENTS

The authors want to thank M. Jose Yacaman for his valuable comments and suggestion on TEM and FE-SEM analyses. This project was financially supported by the Consejo Nacional de Ciencia y Tecnología through grant number 84041.

REFERENCES

1. Hong, F.; Yang, B. L.; Schwartz, L. H.; Kung, H. H. *J. Phys. Chem.* **1984,** *88*, 2525.
2. Woo, K.; Hong, J.; Choi, S.; Lee, H.-W.; Ahn, J.-P.; Kim, C. S.; Lee, S. W. *Chem. Mater.* **2004,** *16*, 2814.
3. Häfeli, U. O.; Riffle, J. S.; Harris-Shekhawat, L.; Carmichael-Baranauskas, A.; Mark, F.; Dailey, J. P.; Bardenstein, D. *Mol. Pharm.* **2009,** *6*, 1417.
4. Babič, M.; Horák, D.; Trchová, M.; Jendelová, P.; Glogarová, K.; Lesný, P.; Herynek, V.; Hájek, M.; Syková, E. *Bioconjugate Chem* **2008,** *19*, 740.
5. Hasegawa, M.; Yanagihara, H.; Toyoda, Y.; Kita, E.; Ranno, L. J. *Magn. Magn. Mater.* **2007,** *310*, 2283.

6. Millan, A.; Palacio, F.; Falqui, A.; Snoeck, E.; Serin, V.; Bhattacharjee, A.; Ksenofontov, V.; Gütlich, P.; Gilbert, I. *Acta Mater.* **2007,** *55*, 2201.
7. Hong, R. Y.; Fu, H. P.; Di, G. Q.; Zheng, Y.; Wei, D. G. *Mater. Chem. Phys.* **2008,** *108*, 132.
8. François, N. J.; Allo, S.; Jacobo, S. E.; Daraio, M. E. *J. Appl. Polym. Sci.* **2007,** *105*, 647.
9. Machala, L.; Zboril, R.; Gedanken, A. J. *Phys. Chem. B* **2007,** *111*, 4003.
10. Lu, Q. H.; Yao, K. L.; Xi, D.; Liu, Z. L.; Luo, X. P.; Ning, Q. J. *Magn. Magn. Mater.* **2006,** *301*, 44.
11. de la Pena O'Shea, V. A.; Álvarez-Galván, M. C.; Campos-Martin, J. M.; Menéndez, N. N.; Tornero, J. D.; Fierro, J. L. *G. Eur. J. Inorg. Chem.* **2006,** *2006*, 5057..
12. Ennas, G.; Musinu, A.; Piccaluga, G.; Zedda, D. *Chem. Mater.* **1998,** *10*, 495.
13. Jeong, J.-R.; Shin, S.-C.; Lee, S.-J.; Kim, J.-D. J. *Magn. Magn. Mater.* **2005,** *286*, 5.
14. Li, Z.; Tan, B.; Allix, M.; Cooper, A. I.; Rosseinsky, M. J. *Small* **2008,** *4*, 231.
15. Pérez, J. A. L.; Quintela, M. A. L.; Mira, J.; Rivas, J.; Charles, S. W. *J. Phys. Chem. B* **1997,** *101*, 8045.
16. Li, J.; Lin, Y.; Zhao, B. J. *Nanopart. Res.* **2002,** *4*, 345.
17. Liu, C.-Y.; Chen, C.-F.; Leu, J.-P.; Lin, Y.-C. J. *Sol-Gel Sci. Technol.* **2007,** *43*, 47.
18. Gorozhankin, D. F.; Eliseev, A. A.; Napol'skii, K. S.; Lukashin, A. V.; Knot'ko, A. V.; Maksimov, Y. V.; Suzdalev, I. P.; Görnert, P.; Tret'yakov, Y. D. *Dokl. Chem.* **2004,** *396*, 132.
19. Hashimoto, S.; Uwada, T.; Masuhara, H.; Asahi, T. J. *Phys. Chem. C* **2008,** *112*, 15089.
20. Rong, M. Z.; Zhang, M. Q.; Wang, H. B.; Zeng, H. M. *J. Polym. Sci. Part B: Polym. Phys.* **2003,** *41*, 1070.
21. Sepúlveda-Guzmán, S.; Lara, L.; Pérez-Camacho, O.; Rodríguez-Fernández, O.; Olivas, A.; Escudero, R. *Polymer* **2007,** *48*, 720.
22. Wetton, R. E.; James, D. B.; US Patent 4,200,701; USA, **1980.**
23. Luna-Martínez J. F., Hernández-Uresti, D. B., Reyes-Melo, M. E., Guerrero-Salazar, C. A., González-González, V. A., Sepulveda-Guzmán, S. *Carbohydr. Polym.* **2011,** *84*, 566.
24. Franco, A. P.; Mercê, A. L. *R. React. Funct. Polym.* **2006,** *66*, 667.
25. Choi, J.-i.; Lee, H. S.; Kim, J.-H.; Lee, K.-W.; Lee, J.-W.; Seo, S.-J.; Kang, K. W.; Byun, M.-W. *Polym. Degrad. Stab.* **2008,** *93*, 310.
26. Cancela, M. A.; Álvarez, E.; Maceiras, R. J. *Food Eng.* **2005,** *71*, 419.
27. ICDD. Powder Diffraction Database, Patter No. 78-075,1 2000.
28. Rajendran, S.; Sivakumar, M.; Subadevi, R. *Solid State Ionics* **2004,** *167*, 335.
29. ICDD. Powder Diffraction Database, Patter No. 39-1346, 2000.
30. ICDD. Powder Diffraction Database, Patter No. 19-0629, 2000.
31. Deng, J.; He, C.; Peng, Y.; Wang, J.; Long, X.; Li, P.; Chan, A. S. *C. Synth. Met.* **2003,** *139*, 295.
32. Gyergyek, S.; Huskić, M.; Makovec, D.; Drofenik, M. *Colloids Surf. A Physicochem. Eng. Aspects* **2008,** *317*, 49.
33. Mukadama, M. D.; Yusufa, S. M.; Sharma, P.; Kulshreshtha, S. K. *J. Magn. Magn. Mater.* **2004,** *272*, 1401.
34. Si, S.; Li, C.; Wang, X.; Yu, D.; Peng, Q.; Li, Y. *Cryst. Growth Des.* **2005,** *5*, 391.
35. Rondinone, A. J.; Samia, A. C. *S.; Zhang, Z. J. J. Phys. Chem. B* **1999,** *103*, 6876.